Low-velocity damaged structure of the San Andreas Fault at Parkfield from fault zone trapped waves

Yong-Gang Li
Department of Earth Sciences, University of Southern California, Los Angeles, California, USA

John E. Vidale and Elizabeth S. Cochran
Institute of Geophysics and Planetary Physics, University of California, Los Angeles, California, USA

Received 10 November 2003; revised 19 March 2004; accepted 29 March 2004; published 18 May 2004.

[1] We used dense linear seismic arrays across and along the San Andreas Fault (SAF) at Parkfield, California to record fault zone trapped waves generated by explosions and microearthquakes in 2002. Prominent trapped waves appeared at stations close to the SAF main fault trace while some energy was trapped in the north strand at the array site. Observations and 3-D finite-difference simulations of trapped waves at 2–5 Hz show evidence of a damaged core zone on the main SAF. The zone from the surface to seismogenic depths is marked by a low-velocity waveguide ~150 m wide, in which Q is 10–50 and shear velocities are reduced by 30–40% from wall-rock velocities, with the greatest velocity reduction at shallow depth. We interpret that this distinct low-velocity zone on the main SAF is a remanent of damage due to past large earthquakes on the principal fault plane at Parkfield. A less-developed low-velocity zone may be evident on the north strand that experienced minor breaks in the 1966 $M6$ event. *INDEX TERMS:* 7200 Seismology; 7209 Seismology: Earthquake dynamics and mechanics; 8123 Tectonophysics: Dynamics, seismotectonics. **Citation:** Li, Y.-G., J. E. Vidale, and E. S. Cochran (2004), Low-velocity damaged structure of the San Andreas Fault at Parkfield from fault zone trapped waves, *Geophys. Res. Lett.*, *31*, L12S06, doi:10.1029/2003GL019044.

1. Introduction

[2] Mature faults are planes of weakness in the Earth crust. Field evidence shows that the rupture plane of slip on a mature fault tends to exist on the edge of a damage zone at the plane of contact with the intact wall rock. At Parkfield, seismological studies have revealed a low-velocity zone surrounding the surface trace of the SAF [e.g., *Lees and Malin*, 1990; *Michelini and McEvilly*, 1991; *Thurber et al.*, 1997]. This zone is a few hundreds of meters to 1 km wide with velocity reductions of 10–30% and Vp/Vs ratios of 2.3. The low Vs and corresponding high Vp/Vs ratios within the fault zone are interpreted to be caused by dilatant fracturing due to high pore-fluid pressures. Magnetotelluric imaging of the SAF at Parkfield yields a similar model, with a zone of very low resistivity a few hundred meters wide extending to a depth of 2–3 km [*Unsworth and Bedrosian*, 2004]; the low-resistivity zone is interpreted to be fluid-rich. *Byerlee* [1990] and *Rice* [1992] note that the high pore-pressures within a fault zone at seismogenic depths may be due in part to its greater permeability than adjacent blocks. Our previous studies at the Parkfield SAF using fault zone trapped waves generated by earthquakes and explosions suggest that the fault zone includes a 100- to 160-m-wide damaged core layer, in which velocities are reduced by 30–40% and Q is ~30 [*Li et al.*, 1990,

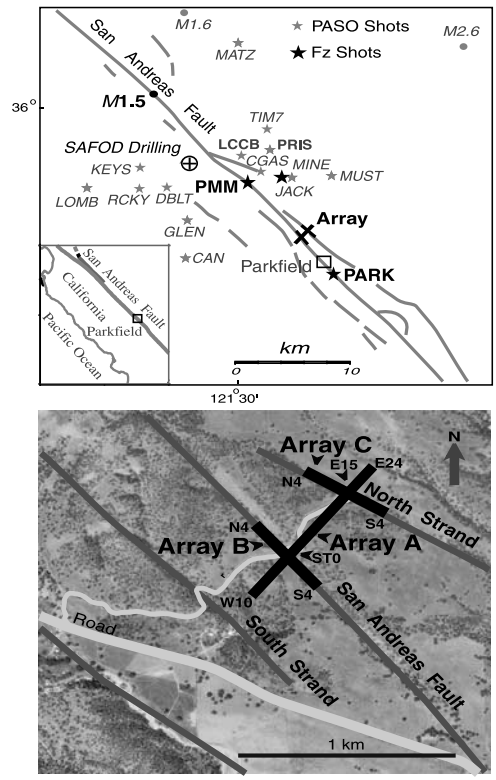

Figure 1. Top: Map shows locations of seismic arrays and shots at Parkfield, California in 2002. Black stars and bars - shots and arrays in fault zone trapped wave study. Grey stars - shots in the PASO experiment. Dots – earthquakes recorded in this study. Bottom: Seismic arrays across and along the SAF. Array A consisted of 35 PASSCAL REFTEKs and 2 Hz L22 sensors with station spacing of 25 m. Arrays B and C consisted of 9 REFTEKs for each with station spacing of 50 m. Stations located at fault traces and ends of arrays are labeled. Grey and white lines are fault surface traces and roads.

0094-8276/04/2003GL019044$05.00

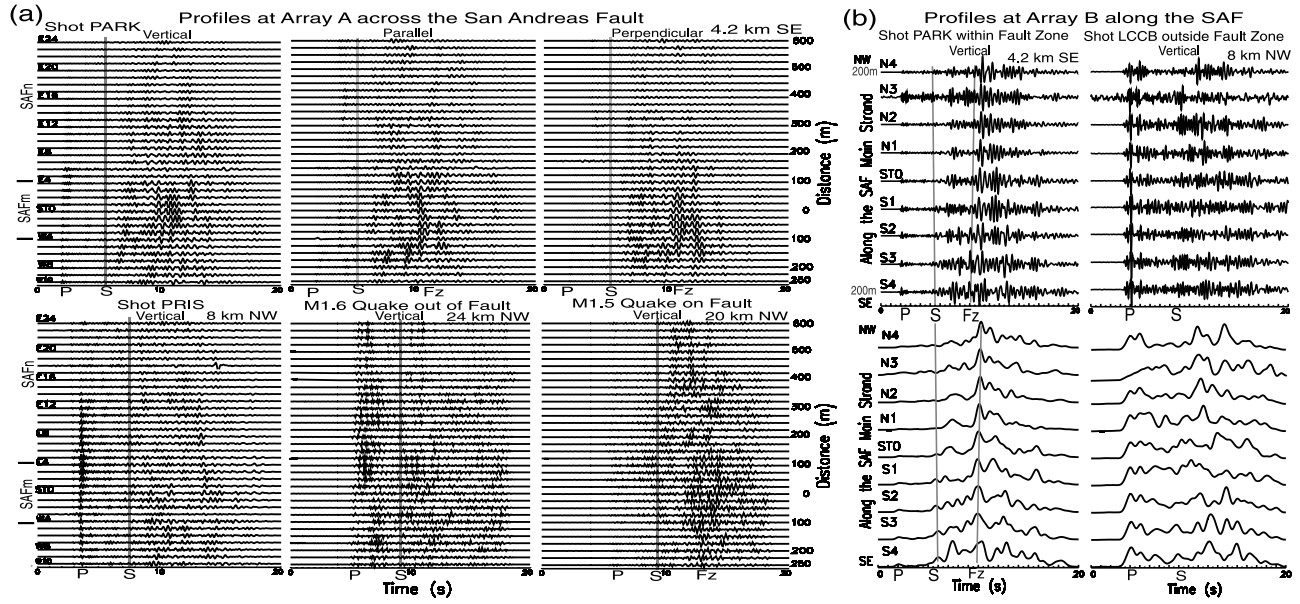

Figure 2. (a) Top: Three-component seismograms recorded at array A for shot PARK. Bottom: Vertical component seismograms at array A for shot PRIS, and *M*1.5 and *M*1.6 earthquakes at Parkfield. The distance between the array and events, station names and offsets are plotted. Stations ST0 and E15 were located on the main fault (SAFm) and north strand (SAFn). Seismograms have been low-pass filtered <4 Hz for shots and <5 Hz for the quake, and are plotted using a fixed amplitude scale for each profile. The shot origin time is at 0 s. Vertical lines are aligned with *S*-arrivals. Fault zone trapped waves (Fz) are dominant at stations in the range marked by two bars for events on the SAF. (b) Vertical component seismograms and computed envelopes at array B for shots PARK and LCCB are trace-normalized in plots. Fault zone trapped waves with large amplitudes appeared after *S* arrivals for shot PARK.

1997]. The data recorded in an extensive experiment at Parkfield in Fall 2002 allow us to characterize the internal structure and damage extent of the fault zone with higher-resolution.

2. Data and Results

[3] We deployed 54 three-component seismometers on 3 dense seismic lines along and across surface traces of the SAF, ~15 km southeast of the drilling site of San Andreas Fault Observatory at Depth (SAFOD), and detonated 3 explosions, each using 250 kilograms of chemical explosives in a 33-m-deep hole, within and outside the fault zone at Parkfield (Figure 1). Array A was 850-m-long across the SAF. Arrays B and C were 400-m along the main and north strands, respectively. The seismic arrays recorded our shots and a dozen smaller shots detonated around the SAFOD drilling site for the PASO experiment [*Thurber et al.*, 2004; *Roecker et al.*, 2004], and 3 earthquakes occurring in the area during 3 weeks of array operation. We observed prominent fault zone trapped waves generated by shots PARK and PMM, and the *M*1.5 earthquake located within the fault zone. For example, Figure 2a shows trapped waves with large amplitudes and long-duration wave trains following *S* waves at stations between E4 and W4 close to the main fault trace for shot PARK and the *M*1.5 quake. The amplitude of trapped waves decreases away from the fault zone. However, trapped waves are not obvious at any station, and *P* waves dominate in the profile for shot PRIS and the *M*1.6 quake at 9-km depth away from the fault. These observations show the existence of a low-velocity waveguide existing on the main fault. The width of waveguide is ~150 to ~200 m between stations E4 and W4 where trapped waves are dominant. Trapped waves from shot PARK traveled slower than those from the *M*1.5 earthquake occurring at 5 km depth and 20 km NW of the array, suggesting that the fault zone has lower velocities at shallower depths. Some trapped energy with a short wave train is noticeable at stations on the north fault strand in the profile for this quake. We infer a weak waveguide with less velocity reduction on the north strand that connects to the main fault at depth NW of the array, and acts to partition some guided energy.

[4] Figure 2b exhibits seismograms recorded at array B along the main fault for shots PARK and LCCB. Trapped waves from shot PARK show coherent phase with large amplitudes after *S* waves in the profile. In contrast, *P* waves dominant in the profile for shot LCCB which was 3 km away from the SAF. In order to eliminate near-surface site effects on fault zone trapped waves, we compute amplitude ratios of trapped waves to *P* waves for the events recorded at the array. The amplitudes are computed in 2 s time windows that include *P* and dominant trapped waves, respectively, from low-pass (<5 Hz) filtered seismograms at all stations. Figure 3 shows the maximum amplitude ratio at the SAF main fault, which decreases rapidly away from the main fault, for events within the fault zone. A second peak is seen at the north strand for the *M*1.5 quake and shot PMM, since the trapped wave energy from them is propagated in the southeast direction and able to partition some energy into the north strand. In contrast, amplitude ratios for events far from the SAF are low and flat across the fault although the low-velocity fault zone is able to trap some seismic energy even if the source locates outside the fault

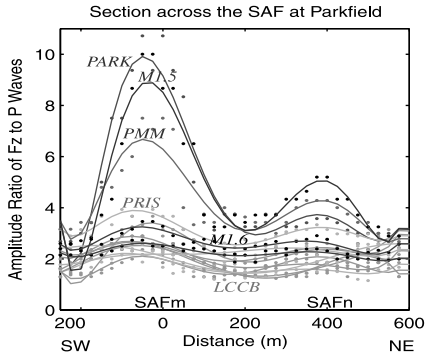

Figure 3. Computed amplitude ratios of fault zone trapped waves to *P* waves at all stations of the 3 arrays for 12 shots and 3 earthquakes versus distance from the main fault trace. Dots are the data points computed from amplitude ratios at all stations of 3 arrays for each event. Curves are a 5th-order polynomial fit to the data for each event. Selected events are labeled. The peak amplitude ratio is seen at stations close to the main fault for events within the fault zone.

zone. Some trapped energy is also seen at the north strand for shot PARK on the main fault.

[5] We modeled the fault zone trapped waves using a 3-D finite-difference code [*Graves*, 1996], resulting in a velocity and *Q* section across the fault to a depth of 5 km, for the structure of the SAF near Parkfield. We first synthesize fault zone trapped waves generated by the near-surface explosions to determine the shallowest 1 or 2 km fault zone structure. We also use velocities from seismic tomography at Parkfield [*Thurber et al.*, 2004] as constraints to the bedrock velocities. We interpret that the later wave train of trapped waves in explosion profiles traveled in the top layer while the early wave train penetrated lower layers. Synthetic seismograms were fit to the later trapped wave train first and then the early trapped wave train was fit in forward modeling. Thus we stripped shallow effects to resolve deeper structure of the fault zone. We then synthesized trapped waves from the earthquake at seismogenic depths to complete a model of the SAF with depth-variable structure in 3-D, including low-velocity waveguides on the main and north fault strands (Figures 4a and 4b). We also use

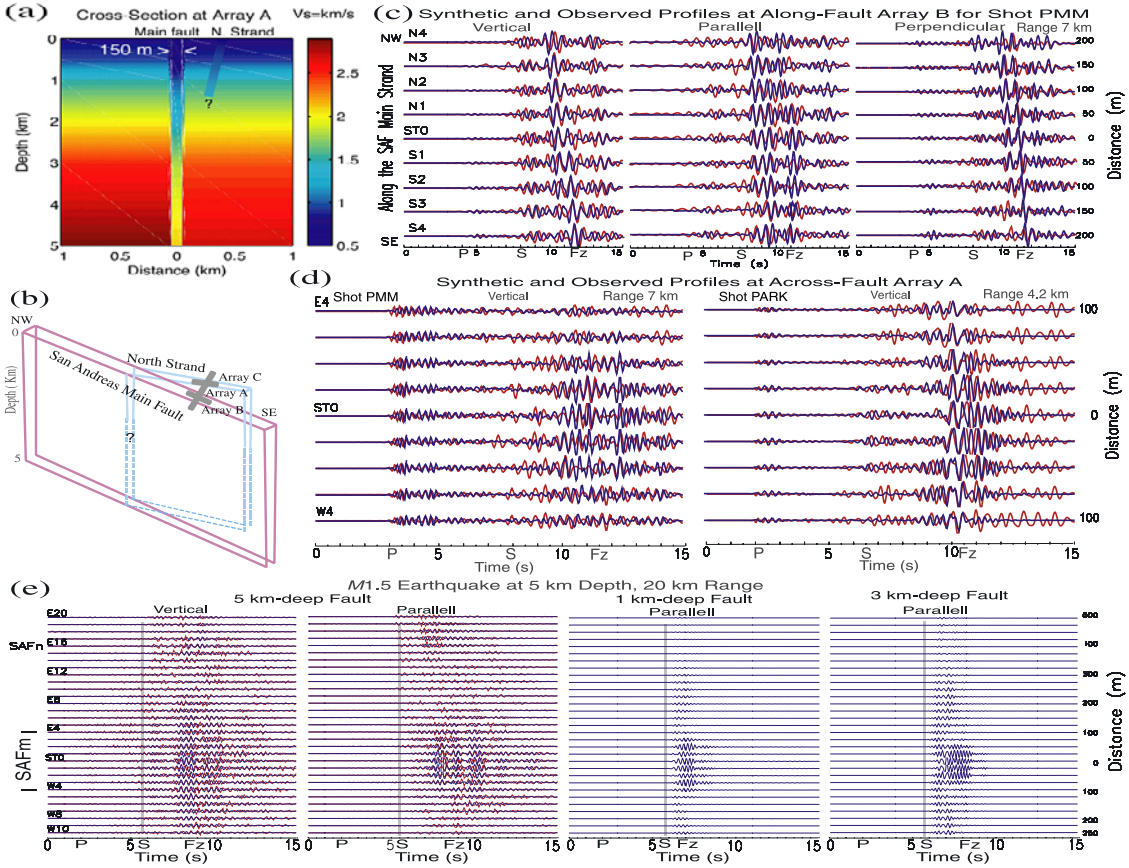

Figure 4. (a) Depth section of *S* velocities across the SAF at the array site. The main fault is marked by a ~150-m-wide waveguide in which velocities are reduced by 30–40% and *Q* is 10–50 between the surface and 5 km depth. The north strand is marked by a minor waveguide. (b) The schematic fault planes at depths in the study area. (c) Observed (red lines) and synthetic (blue lines) seismograms at array B for shot PMM. Seismograms have been low-pass (<3 Hz) filtered and are trace-normalized in plots. An explosion source is located within the waveguide. (d) Same as in (c), but at 9 stations of array A close to the main fault for shots PMM and PARK. Seismograms are plotted using a fixed amplitude scale in each profile. (e) Same as in (d), but at array A for the *M*1.5 earthquake. A double-couple source was located at the 5 km depth within the waveguide. Synthetic seismograms for 1- and 3-km-deep shallow fault zones are shown for comparison with those for the 5-km-deep fault zone.

Table 1. Parameters for the SAF Near Parkfield

Parameters Layer No.	1	2	3	4
Main fault NW/SE of array A:				
Depth of the layer, km	0.25	1.0	2.0	5.0
Waveguide width, m	175/150	175/150	150/125	125/100
Waveguide *Vs*, km/s	0.5/0.35	0.65/0.55	1.0/0.9	1.7/1.4
Waveguide *Vp*, km/s	1.3/1.0	1.8/1.4	2.3/2.1	3.5/3.0
Waveguide *Q*	10	25	30	50
NE wall-rock *Vs*, km/s	0.8/0.6	1.0/0.9	1.5/1.4	2.3/2.0
NE wall-rock *Vp*, km/s	2.0/1.5	2.5/2.2	3.3/3.0	5.0/4.2
SW wall-rock *Vs*, km/s	0.8/0.6	1.0/0.9	1.6/1.5	2.5/2.2
SW wall-rock *Vp*, km/s	2.0/1.5	2.5/2.2	3.5/3.2	5.2/4.5
Wall rock *Q*	20	50	60	100
North fault strand:				
Waveguide width, m	50	50	50	50
Waveguide *Vs*, km/s	0.65	0.8	1.3	2.0
Waveguide *VP*, km/s	1.6	2.0	2.8	4.0
Waveguide Q	30	40	50	

velocities from seismic tomography at Parkfield [*Thurber et al.*, 2004] as constraints to the bed-rock velocities. In grid-search modeling, we tested various values for fault zone width, velocity, *Q*, layer depth, and source location. The best-fit model parameters are shown in Table 1.

[6] Figure 4c exhibits observed and synthetic seismograms at the along-fault array B for shot PMM. Fault zone trapped waves with large amplitudes, long duration, and slightly dispersive wave trains follow *S* waves. Figure 4d shows observed and synthetic seismograms at 9 stations of array A close to the SAF main fault for shots PMM and PARK. Fault zone trapped waves are dominant at these stations. Figure 4e exhibits observed and synthetic seismograms at array A for the *M*1.5 quake occurring at the 5 km depth within the SAF. Trapped waves are seen clearly at the main fault. Some trapped energy with smaller amplitudes and shorter wave trains appeared at the north strand. The waveform cross-correlations between observed and synthetic seismograms computed in a 3 s time window covering the dominant trapped-waves show that the correlation coefficient is 0.8–0.9 at stations close to the main fault, but is lower at stations far from the fault and in the later coda. We tested various fault zone depths in modeling. For example, synthetic seismograms generated by the *M*1.5 event for a 3-km-deep low-velocity fault zone show the longer duration than that for a 1-km-deep fault zone. However, they can not match observed guided waves with longer wave trains after *S* waves.

3. Discussions and Conclusions

[7] Through fault zone trapped wave data collection and analysis, we quantitatively characterize the dimensions and magnitude of the highly damaged core zone on the SAF at Parkfield. The zone on the main fault is marked by a low-velocity waveguide ~150 m wide, in which *Q* is 15–50 and *S* velocities are reduced by 30–40% from wall-rock velocities, varying with depth and along the fault. Trapped waves recorded for a microearthquake at 5 km depth within the fault zone suggest that the low-velocity waveguide may extend to that depth. In our experiment in 2002, we recorded only 3 earthquakes in the Parkfield area. Additional deeper events are necessary to document the depth extent of the fault zone more quantitatively. The structural model presented in Figure 4a is a simple and plausible one that explains much of the data but the true structure may be considerably more complicated, and we are striving for the data to elucidate it. The coincidence of low seismic velocity, high conductivity and Poisson's ratio [*Thurber et al.*, 2003; *Unsworth et al.*, 1997] suggests that a zone of fluid saturated fractured rock associated with the SAF may extend to the depth of up to ~5 km, although recent analyses of magnetotelluric data indicate that the fault zone conductor at Parkfield is probably about 2–3 km deep [*Unsworth and Bedrosian*, 2004]. In comparison, only a 3-km-deep low-velocity zone is reported on the rupture of the 1999 M7.5 Izmil earthquake [*Ben-Zion et al.*, 2003]. We interpret that the distinct low-velocity core zone was formed by repeated damage during recurrent *M*6 earthquakes and other large events on the principal slip plane at Parkfield. A less-developed narrower low-velocity zone may exist on the north strand at the array site, which experienced minor surface breaks in the 1966 *M*6 event, most likely due to secondary slip and strong shaking from ruptures on the main fault. The width of the low-velocity waveguide inferred by trapped waves likely represents the macroscopic damage extent in dynamic rupture and microscopic fault process zone accumulating mechanical, chemical, thermal, and other kinematical processes. The variation in velocity reduction along the fault zone and with depth may be caused by changes in overburden pressure, rock type, stress and slip rate, fault geometry, fluid content, and dynamic rupture during past earthquakes.

[8] **Acknowledgments.** This study was supported by NSF/Pre-EarthScope Grant EAR-207214 and partially by the SCEC. Special thanks to SAFOD PIs for their coordination of our experiment, and J. Varian, J. Cocker and W. Mosby for permissions to conduct experiment on their lands. We are grateful to C. Thurber and S. Roecker for PASO shots, the IRIS for the use of PASSCAL instruments, and T. Burdette with other shooters of the USGS for detonation of explosions. We thank Editor A. Zollo, C. Marone, and an anonymous reviewer for helpful comments on the manuscript. The SCEC contribution number of this paper is 762.

References

Ben-Zion, Y., Z. Peng, D. Okaya, L. Seeber, J. Armbruster, N. Ozer, A. Michael, S. Baris, and M. Aktar (2003), A shallow fault zone structure illuminated by trapped waves in the Karadere-Duzce branch of the North Anatolian Fault, western Turkey, *Geophys. J. Int.*, *152*, 699–717.

Byerlee, J. (1990), Friction, overpressure and fault-normal compression, *Geophys. Res. Lett.*, *17*, 2109–2112.

Catchings, R. D., M. J. Rymer, M. R. Goldman, J. A. Hole, R. Huggings, and C. Lippus (2002), High-resolution seismic velocities and shallow structure of the San Andreas Fault zone at Middle Mountain, Parkfield, California, *Bull. Seismol. Soc. Am.*, *92*, 2493–2503.

Graves, R. W. (1996), Simulating seismic wave propagation in 3D elastic media using staggered-grid finite differences, *Bull. Seismol. Soc. Am.*, *86*, 1091–1106.

Lees, J. M., and P. E. Malin (1990), Tomographic images of *P* wave velocity variation at Parkfield, California, *J. Geophys. Res.*, *95*, 21,793–21,804.

Li, Y. G., P. C. Leary, K. Aki, and P. E. Malin (1990), Seismic trapped modes in Oroville and San Andreas Fault zones, *Science*, *249*, 763–766.

Li, Y. G., W. L. Ellsworth, C. H. Thurber, P. E. Malin, and K. Aki (1997), Observations of fault-zone trapped waves excited by explosions at the San Andreas Fault, central California, *Bull. Seismol. Soc. Am.*, *87*, 210–221.

Michelini, A., and T. V. McEvilly (1991), Seismological studies at Parkfield, I, Simultaneous inversion for velocity structure and hypocenters using cubic B-splines parameterization, *Bull. Seismol. Soc. Am.*, *81*, 524–552.

Rice, J. R. (1992), Fault stress states, pore pressure distributions and the weakness of the San Andreas Fault, in *Fault Mechanics and Transport Properties of Rocks*, edited by B. Evans and T.-F. Wong, pp. 475–503, Academic, San Diego, Calif.

Roecker, S., C. Thurber, and D. McPhee (2004), Joint inversion of gravity and arrival time data from Parkfield: New constraints on structure and

hypocenter locations near the SAFOD drill site, *Geophys. Res. Lett.*, *31*, L12S04, doi:10.1029/2003GL019396.

Thurber, C., S. Roecker, K. Roberts, M. Gold, L. Powell, and K. Rittger (2003), Earthquake location and three-dimensional fault zone structure along the creeping section of the San Andreas fault near Parkfield, CA: Preparing for SAFOD, *Geophys. Res. Lett.*, *30*, 1112, doi:10.1029/2002GL016004.

Thurber, C., S. Roecker, H. Zhang, S. Baher, and W. Ellsworth (2004), Fine-scale structure of the San Adreas fault zone and location of the SAFOD target earthquakes, *Geophys. Res. Lett.*, *31*, L12S02, doi:10.1029/2003GL019398.

Unsworth, M., and P. A. Bedrosian (2004), Electrical resistivity at the SAFOD site from magnetotelluric exploration, *Geophys. Res. Lett.*, *31*, L12S05, doi:10.1029/2003GL019405.

Unsworth, M., P. Malin, G. Egbert, and J. Booker (1997), Internal structure of the San Andreas Fault at Parkfield, CA, *Geology*, 356–362.

E. S. Cochran and J. E. Vidale, IGGPP, University of California, Los Angeles, Los Angeles, CA 90095, USA.

Y.-G. Li, Department of Earth Sciences, University of Southern California, Los Angeles, CA 90089, USA. (ygli@usc.edu)